Transactions of the SMiRT 27
Yokohama, Japan, March 3-8, 2024
Division 1

TEM characterization of microstructure and radiation-induced defects in western PWR model steels with varying Ni and Mn contents and correlation to mechanical properties

V.S.M. Pereira[1], F. Naziris[2], S.P.A. Hageman[3], T. Holvast[4], I. Szenthe[5], D. Cinger[6], E. D'Agata[7], N.V.V.R.M. Kolluri[8]

[1] Research Scientist (PhD), Nuclear Research & consultancy Group (NRG), Petten, The Netherlands (marques@nrg.eu)
[2] Research Scientist (MSc), Nuclear Research & consultancy Group (NRG), Petten, The Netherlands
[3] Research Scientist (BSc), Nuclear Research & consultancy Group (NRG), Petten, The Netherlands
[4] Research Scientist, Nuclear Research & consultancy Group (NRG), Petten, The Netherlands
[5] Research Scientist (MSc), Centre for Energy Research, Budapest, Hungary
[6] Research Scientist (MSc), Centre for Energy Research, Budapest, Hungary
[7] Research Scientist (PhD), European Commission - Joint Research Centre (JRC), Directorate G – Nuclear Safety & Security, Petten, The Netherlands
[8] Research Scientist (PhD), Nuclear Research & consultancy Group (NRG), Petten, The Netherlands

ABSTRACT

The present paper contains preliminary results of an ongoing effort to characterize the microstructure and defect structure of western PWR RPV model steels, as part of the scope of the STRUMAT-LTO project. The materials are low-Cu PWR model steels, with systematic variations in Ni and Mn contents and were studied in reference, irradiated and post-irradiated annealed at 450 ºC for 40 h conditions. SEM and TEM were used to characterize the general microstructure and nanofeatures in the materials, respectively. Vickers hardness measurements were performed on specimens in reference and irradiated conditions and, as expected, show that the materials undergo irradiation embrittlement. Microscopy analyses show that the steels have complex microstructures in the reference condition, composed of martensitic/bainitic matrix, Fe-rich sub-micrometric precipitates at grain boundaries and Mo-rich nanosized precipitates (~15 to 150 nm length) located inside grains. In the irradiated condition, it was not possible to image dislocation loops, which are expected to form with sizes of approximately 4 nm in this kind of material. Instead, a surprising increase in the amount of Mo-rich nanosized precipitates was observed after irradiation. For most part of the steel grades analyzed, the PIA treatment did not lead to microstructural changes resolvable with the TEM, although in previous work, the treatment was effective in recovering the mechanical properties.

INTRODUCTION

One of the limiting factors of long-term operation (LTO) of LWRs is the ageing of the reactor pressure vessel (RPV). The latter needs to maintain sufficient ductility throughout its service life for normal operation conditions and to withstand possible accidental-like situations (e.g. pressurized thermal shock). Embrittlement due to neutron irradiation is the main factor affecting the ductility and thus integrity of the RPV. Typical materials used in RPVs of LWRs are low-alloy steels containing Mn, Mo, Ni, Si and Cr and, as impurities, Cu and P. Already in the mid-1990s, studies predicted the formation of Mn-Ni-(Si) phases in low-Cu steels at low nucleation rates and high incubation fluences (Odette & Lucas, 1998), (Odette, 2009). These so-called "late blooming" phases lead to a substantial increase in the embrittlement for high fluence values, relevant to LTO (Almirall, et al., 2019), (Bonny, et al., 2013). The lack of systematic investigation in the past makes it difficult to draw consistent conclusions regarding the individual and synergetic effect of elements such as Ni, Mn and Si on the irradiation-induced degradation mechanisms of RPV, especially for the high fluence range. Thus, one of the aims of the Euratom-funded project "STRUctural MATerials research for safe Long Term Operation of LWR nuclear power plants", STRUMAT-LTO, is to improve the understanding of the role of Ni, Mn and Si on irradiation embrittlement of RPV steels. More detailed information about the project can be found in (Kolluri, 2023).

Different specimens made of various RPV model steels, based on western pressurized water reactors (PWR) and VVER-1000 RPV base metal steels, and realistic welds based on VVER-1000 RPV high-Ni weld steel were irradiated to high fluences in the High Flux Reactor (HFR) in Petten, The Netherlands within the joint NRG-JRC irradiation campaign LYRA-10. Several partners are responsible for the extensive post-irradiation examination (PIE) campaign, constituted of varied mechanical testing (tensile, Charpy impact tests, fracture toughness, Small Punch testing, Vickers hardness) and thorough characterization of microstructure and radiation-induced defects, using complementary techniques like Scanning Electron Microscopy, Transmission Electron Microscopy, Atom Probe Tomography, Small Angle Neutron Scattering, Positron Annihilation Spectroscopy, among others. In addition, part of the irradiated specimens were submitted to post-irradiation annealing treatment at 450 ºC for 40 h, in order to investigate its effectiveness to recovering mechanical properties and its potential use as mitigation strategy for LTO of RPVs (Laot, et al., 2022).

The present paper contains preliminary results of the ongoing effort to characterize the microstructure and radiation-induced defects formed during the LYRA-10 irradiation, as well as their thermal evolution with the performed PIA at 450 ºC for 40 h. A combination of SEM, TEM, dilatometry and Vickers hardness is used, in an attempt to correlate microstructure to mechanical testing results published previously by (Kolluri, et al., 2021) and (Laot, et al., 2022).

EXPERIMENTAL

The materials studied are the PWR model steels K, L, M and N, produced with chemical compositions similar to A508 Cl. 2 (1989) steel, with varying Ni and Mn contents. The steels were fabricated according to the following route: casting, forging, hot rolling at 1180 ºC and subsequent thermal treatments for obtaining microstructures composed of a martensite/bainite mixture. Afterwards, the steel plates were further heat treated with the aim of obtaining the yield strength $R_{p0.2}$ = 550 ± 30 MPa for all grades at room temperature. These final treatments consisted of (1) isothermal treatment at 640 ºC for 10 h in air atmosphere, followed by (2) austenitization at 940 ºC for grade K and at 900 ºC for grades L, M and N, with holding time of 20 min, and subsequent water quench and (3) a final tempering stage of the as-quenched microstructures at 640 ºC, in air atmosphere, for holding times of 12 h (grades K and L), 10 h (grade M) and 20 h (grade N), and subsequential air cooling.

Specimens of steel grades K, L, M and N were irradiated in the LYRA-10 experiment, carried out by NRG and JRC at the HFR, Petten, as part of the STRUMAT-LTO project. The duration of the irradiation campaign was 16 HFR cycles, which correspond to ~467 full-power days. The average irradiation temperature was 286 ºC and a nominal fast neutron fluence of 1.1 x 10^{20} $n.cm^{-2}$ was achieved. The nominal dpa of the samples is 0.18. More detailed information about the LYRA-10 irradiation can be found in (Kolluri, et al., 2021). After irradiation, part of the specimens were annealed at 450 ºC for 40 h, with the objective of investigating the efficiency of this post-irradiation annealing (PIA) treatment on the recovery of mechanical properties. The PIA treatment was conducted in an electrical SEVERN SF835 furnace, and the samples were cooled inside the furnace (Laot, et al., 2022).

Table 1 Chemical composition of the four grades of PWR RPV model steels studied in the project STRUMAT-LTO.

Chemical composition in weight % of PWR RPV model steels									
Grade	C	Si	Mn	Cr	Ni	Mo	Cu	S	P
K	0.170	0.350	0.780	0.100	0.580	0.640	0.070	0.005	0.009
L	0.180	0.350	0.770	0.080	0.960	0.630	0.050	0.005	0.010
M	0.160	0.370	0.740	0.090	1.900	0.610	0.050	0.005	0.010
N	0.160	0.330	1.270	0.070	1.970	0.630	0.060	0.005	0.010

In order to gain more insight into the phase transformation behaviour of the model steels K, L, M and N, dilatometry tests were conducted in a Bahr DIL805A/D dilatometer. Broken mini-Charpy (KLST) specimens in reference condition, tested previously within the STRUMAT-LTO scope, were transformed in dilatometry samples by laser-cutting their fracture surfaces, thus resulting in small beams

with dimensions 3 x 4 x 10 mm^3. The heat treatments (2) and (3) described in the "Materials" section were almost entirely reproduced in the dilatometer, with the only difference being the duration of the tempering step, which was reduced to 1.5 h. Figure 1 is a schematic illustrating the heat treatments performed in the dilatometer.

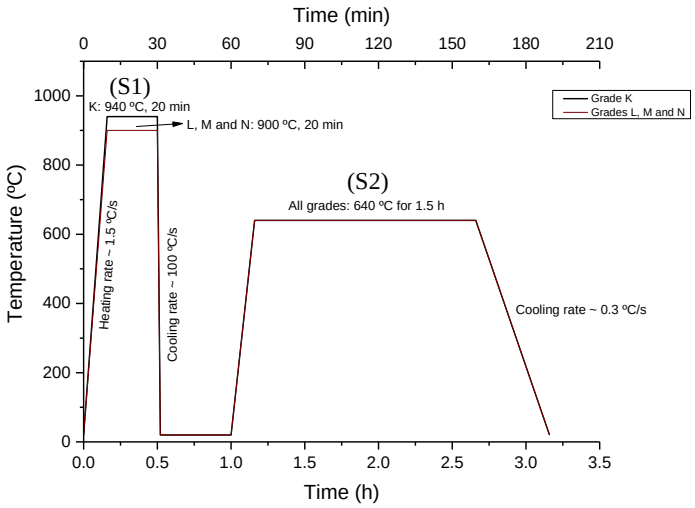

Figure 1. Schematics of heat treatments performed in model steel grades K, L, M and N, in reference condition, during dilatometry measurements.

Microstructural characterization was conducted in the PWR model steels K, L, M and N in the following conditions: (i) reference, (ii) irradiated, (iii) PIA at 450 ºC for 40 h and (iv) dilatometry-tested. Scanning Electron Microscopy was used for observing the general microstructure (matrix, sub-micrometric precipitates) in conditions (i) and (iv), while Transmission Electron Microscopy was used to image nanosized features present in the steels in conditions (i), (ii) and (iii). SEM analyses were performed in a Hitachi S-3700N and in a JEOL 6500FD; TEM investigations were carried out in a JEOL JEM-1200ex, operating at 120 kV and, partially, in a JEOL-JEM2010 operating at 200 kV (only grades K and N, in reference condition). Samples for microscopy analysis of conditions (i), (ii) and (iii) were extracted from grips of broken tensile and mini-Charpy (KLST) specimens, studied previously by (Kolluri, et al., 2021) and (Laot, et al., 2022), as part of STRUMAT-LTO project.

Quantification of observed features was made using the software *ImageJ* and in accordance with ASTM E1245-30 standard. The volume fraction and particle size distribution of sub-micrometric and micrometric features were estimated using secondary electron micrographs obtained with the SEM. A total of 2 images per grade, in reference condition, were used and the particles were approximated as spheres. The particle size distribution and planar density (particles.m^{-2}) of nanosized features present in the steels (reference, irradiated and PIA conditions) were calculated using bright field micrographs obtained with the TEM. In this case, an average of 10 images per condition were analysed and particle size was considered to be the Feret diameter.

Finally, Vickers hardness measurements were performed on all grades in conditions (i) reference, (ii) irradiated and (iv) dilatometry-tested. For testing of conditions (i) and (ii), an INNOVATEST Falcon 500 hardness device was used and the load applied was 1 kgf. A minimum of 3 specimens per grade were measured and 5 indentations per specimen were taken.

RESULTS AND DISCUSSION

The dilatometry measurements during the austenitization step, indicated as S1 in Figure 1, allowed for determination of Ac_1, Ac_3 and M_s temperatures of the model steels K, L, M and N, with Ac_1 = temperature at which ferrite starts to transform in austenite, Ac_3 = temperature at which austenitization is completed and M_s = temperature at which martensite starts to form, upon cooling from the austenitic field. For grade K, Ac_1 = 742 ºC, Ac_3 = 872 ºC and M_s = 389 ºC; for grade L, Ac_1 = 736 ºC, Ac_3 = 868 ºC and M_s = 399 ºC; for grade M, Ac_1 = 719 ºC, Ac_3 = 828 ºC and M_s = 381 ºC; for grade N, Ac_1 = 728

ºC, Ac_3 = 816 ºC and M_s = 376 ºC. After quenching from S1, the resulting microstructures of the steels are composed of fresh martensite and, hence, step S2 consists of tempering of fresh martensite.

The dilatometry curves measured during the tempering step, indicated as S2 in Figure 1, are shown in Figure 2. The tempering and first derivative curves are very similar for the four model steels; only the tempering curve measured for steel grade L begins at lower "change in length" values, likely due to more contraction of the specimen during quenching from S1, but its profile is similar to the observed for other grades. Figure 2 shows that all steels exhibit a small "lump" in the heating portion of the tempering curve, between 300 ºC and 400 ºC. The curves of first derivative of change in length *vs* temperature show, in accordance to the tempering curves, a first inflection point at 300 ºC (seen as a peak), which likely marks the start of a microstructural process. At 400 ºC, another inflection point is present (seen as a valley), which indicates the end of the same microstructural process. The microstructural process in question is likely the precipitation of second-phase particles, expected to occur during tempering of martensite. The obtained first derivative curves seen in Figure 2 are all very irregular, possibly due to the heating rate of 1.5 ºC/s applied, higher than what is normally used for studying tempering of martensite (0.083 ºC/s, as in (Waterschoot, et al., 2006)).

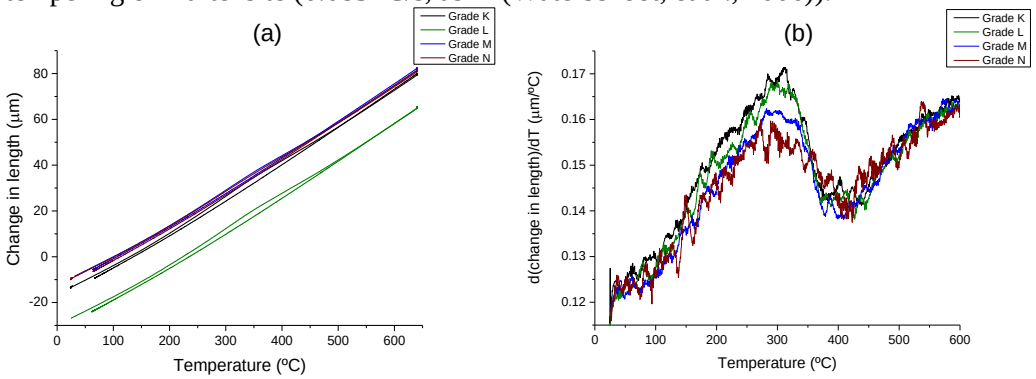

Figure 2. Dilatometry curves of (a) change in length *vs* temperature and (b) first derivative of change in length *vs* temperature obtained for model steels K, L, M and N during tempering.

The microstructures of model steels K, L, M and N in conditions (i) reference and (iv) dilatometry-tested are presented in Figures 3 and 4, respectively. As a reminder, the final heat treatment applied during fabrication of the model steels and, therefore, for the creation of the reference condition (i) were tempering at 640 ºC for 12 h (grades K and L), 10 h (grade M) and 20 h (grade N). The tempering stage S2 during dilatometry was carried out at 640 ºC for 1.5 h.

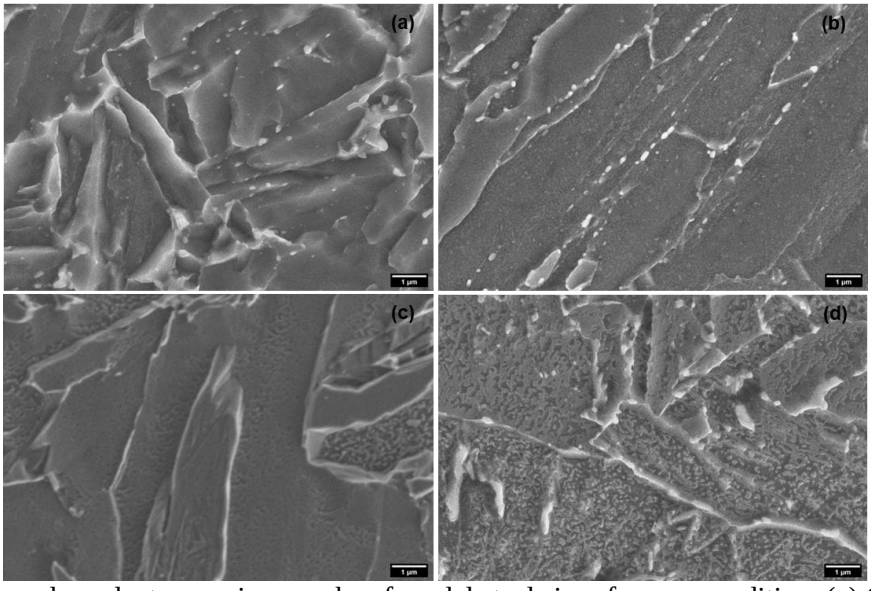

Figure 3. Secondary electrons micrographs of model steels in reference condition. (a) Grade K, (b) grade L, (c) grade M, (d) grade N.

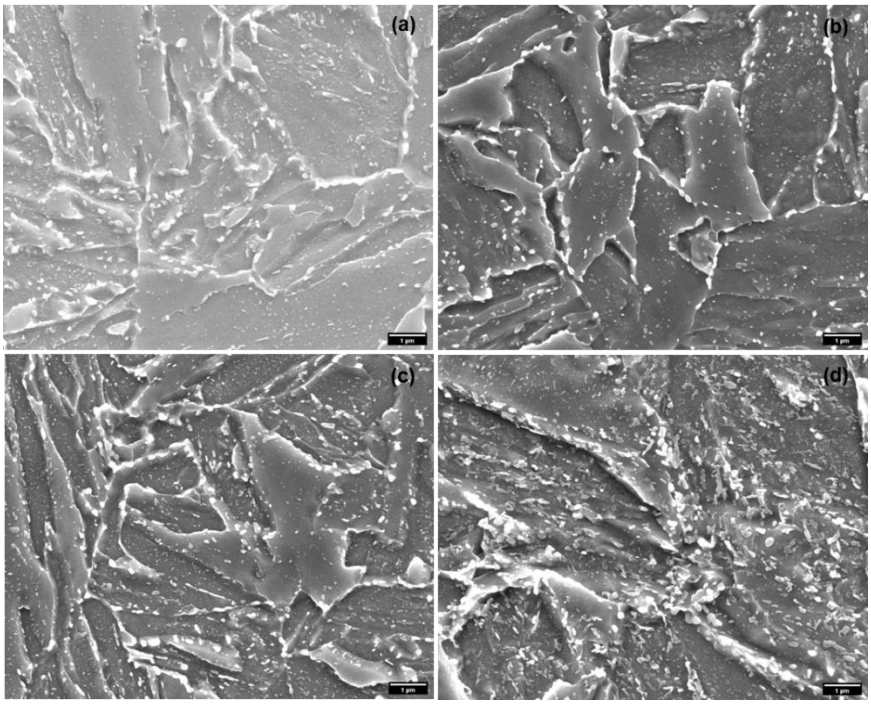

Figure 4. Secondary electrons micrographs of model steels in dilatometry-tested condition, with final tempering stage at 640 ºC and holding time (t_h) of 1.5 h. (a) Grade K, (b) grade L (c) grade M and (d) grade N.

The matrixes of the model steels K, L, M and N are composed of mixtures of tempered martensite and bainite. Figure 3 shows that, in reference condition, sub-micrometric precipitates are present in grain boundaries in steels K, L and N, whereas steel M does not show any precipitated particle at grain boundaries. The estimated volume fractions of grain boundary precipitates in model steel grades K, L and N, in reference condition, are 3%. Interestingly, Figure 4 shows that the microstructures of model steels K, L, M and N, obtained after a shorter tempering time, present a significantly higher volume fraction of grain boundary precipitates, and it is also possible to see finer precipitates inside grains. These results suggest that precipitates likely formed between 300 ºC and 400 ºC during tempering, are not thermally stable when exposed to 640 ºC: their dissolution occurs as tempering time progresses. However, the reason for highest dissolution rate in grade M is unclear, since the chemical compositions of all model steels are virtually the same, except for the variation in Mn and Ni.

Figures 5, 6 and 7 contain bright field micrographs of model steel grades K, M and N, respectively, in reference, irradiated and PIA at 450 ºC for 40 h conditions. The results obtained for grade L are not shown in the present paper due to its high similarity to grade K.

Analysis of the model steels in reference condition showed the presence of nanosized precipitates inside grains. Some nanosized precipitates present needle-like morphology, while others are approximately spherical. Dark field micrographs and EDS analyses (not shown in the present paper) indicate that all of them are Mo-rich carbides and, therefore, the morphologies observed are due to different orientations of these precipitates within grains. In addition, further EDS analyses showed that the sub-micrometric precipitates present at grain boundaries of model steels K, L and N consist of Fe-rich carbides, with a Mn content of around 5 weight%. Figure 8 shows the size distributions calculated for the nanosized Mo-rich precipitates in the model steel grades K, M and N (grade L is not shown due to similarity with grade K) and their respective planar densities in all investigated conditions.

The evaluation of the model steels in irradiated condition revealed unexpected results. First, it was not possible to visualise any dislocation loops in the materials. Second, an increase in the amount of nanosized Mo-rich carbides was observed in grades K, L and M after irradiation. In fact, grade M in irradiated condition shows Fe-rich sub-micrometric precipitates at grain boundaries (Figure 6(c)), not encountered in the reference condition. Finally, qualitatively, no significant differences can be observed

between irradiated and PIA conditions, for grades K, L and N; for grade M, post-irradiation annealing at 450 ºC for 40 h leads to the dissolution of the Fe-rich grain boundary precipitates (Figure 6(e)).

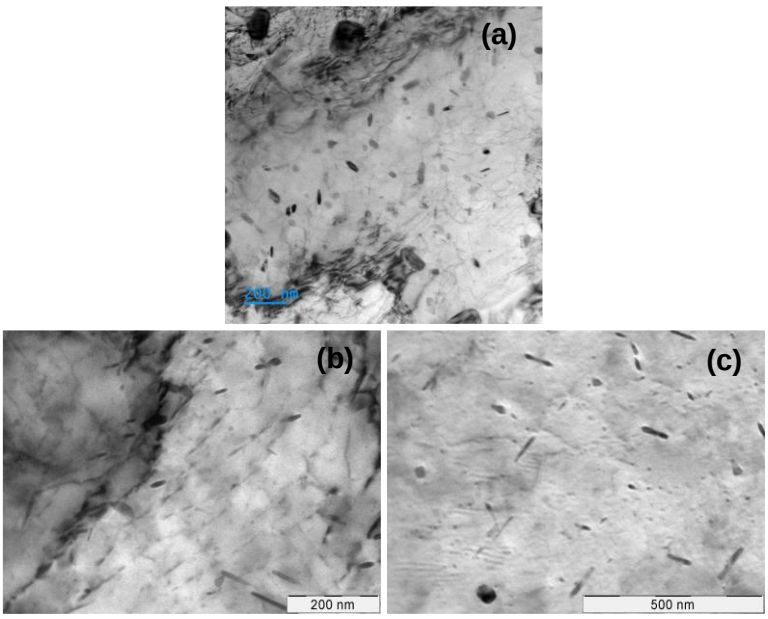

Figure 5. Bright field micrographs of model steel grade K in different conditions. (a) Reference, (b) irradiated and (c) post-irradiation annealed at 450 ºC for 40 h.

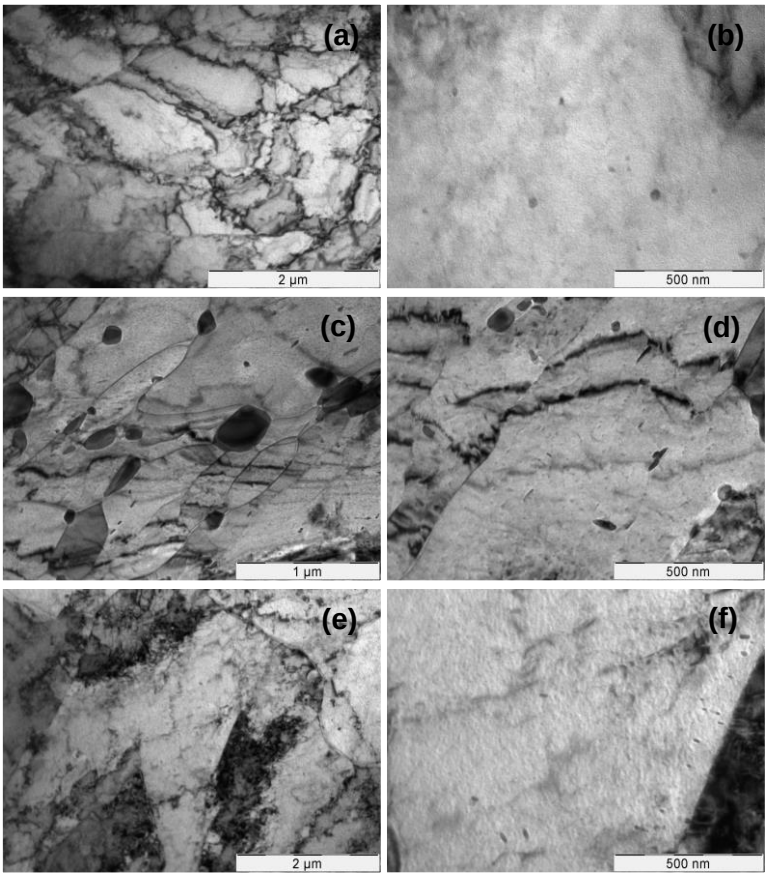

Figure 6. Bright field micrographs of model steel grade M (a) and (b) reference, (c) and (d) irradiated, (e) and (f) post-irradiation annealed at 450 ºC for 40 h

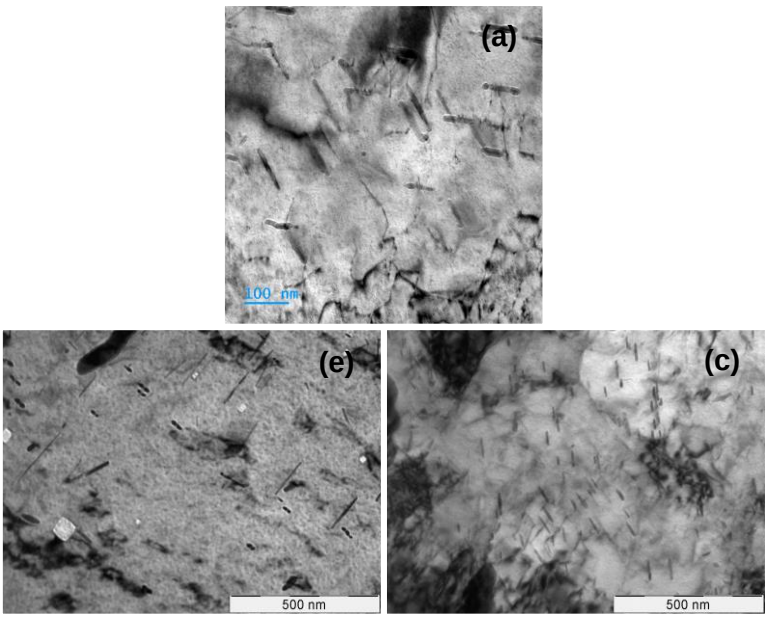

Figure 7. Bright field micrographs of model steel grade N in different conditions. (a) Reference, (b) irradiated and (c) post-irradiation annealed at 450 ºC for 40 h.

The particle size distributions in Figure 8 show an increased fraction of particles with 10-20 nm for all steels in irradiated condition, in comparison to reference condition, accompanied by an increased planar density of particles. It can also be seen that, for grades K and N, the particle size distribution does not change after PIA at 450 ºC for 40 h. For grade M, the PIA at 450 ºC for 40 h not only led to the dissolution of grain boundary precipitates, but also made the size distribution of Mo-rich particles similar to the calculated for the reference condition. The planar density values determined for grade N in reference, irradiated and PIA conditions (Figure 8(d)) show a high standard deviation, due to existence of microstructural banding in the material. The banded regions present higher fraction of Mo-rich precipitates than regions without banding.

In relation to the non-observation of dislocation loops during analysis of the irradiated specimens, two considerations need to be taken into account: one is the limitation with the TEM used, which operates at 120 kV, and the second is the high density of nanosized solute clusters rich in Ni, Mn and Si, expected to form in this kind of alloy (Almirall, et al., 2019), (Shimodaira, et al., 2018), (Wells, et al., 2014). The sizes of dislocation loops in low-Cu RPV steels, like the model steels K, L, M and N, irradiated to neutron fluences similar to the achieved during the LYRA-10 experiment, are expected to be of around 4 nm, or less (Fujita, et al., 2022), (Shimodaira, et al., 2018). The image resolution obtained with the 120 kV TEM is much decreased, compared to microscopes operating at 200 kV that are more modern. Attempts to image dislocation loops by using Dark Field and Weak Beam Dark Field (WBDF) were also made, but without success. In a next phase of the project the samples will be reanalysed in a TEM operating at 200 kV, with focus on WBDF to image dislocation loops. Regarding the formation of solute clusters during irradiation, which cannot be imaged with TEM, it has been discussed in literature that solute clusters are associated to dislocation loops and self-interstitial atoms (SIA) in low-Cu steels (Fujita, et al., 2022). Hence, it is possible that a fraction of dislocation loops in K, L, M and N steels are associated with Mn-Ni-Si solute clusters, being hindered to grow to sizes resolved by the TEM.

The observation of higher density of nanosized Mo-rich precipitates, with dimensions ranging from 10 to 20 nm, in irradiated specimens (Figure 8), compared to the reference condition, is odd. It has been discussed in Figure 2 the formation of precipitates between 300 ºC and 400 ºC in the K, L, M and N model steels, during tempering of fresh martensite. The target irradiation temperature in the LYRA-10 experiment was 290 ºC, close to the precipitation temperature suggested by the dilatometry measurements. However, it is unlikely that Mo-rich precipitates are forming at such low temperatures, even when considering the un-irradiated condition. A more detailed study of the precipitation behaviour of model steels K, L, M and N is needed in order to better understand the presence of higher density of

these Mo-rich precipitates in irradiated condition. On the other hand, the observation of sub-micrometric Fe-rich precipitates on the irradiated model steel M, can be explained by results presented in Figures 2-4. Tempering at 640 ºC for 10 h leads to the complete dissolution of Fe-rich precipitates located at grain boundaries in grade M. Therefore, during irradiation at 290 ºC re-precipitation of the Fe-rich particles occurs. Nevertheless, the reason for the lower thermal stability of precipitates in grade M is unclear, since the chemical composition of the model steels is virtually the same, except for the variation in Ni and Mn contents, and needs to be further evaluated.

Figure 9 contains the Vickers hardness results obtained for the K, L, M and N steels measured in reference and irradiated conditions. As expected, after irradiation, the hardness of the materials is increased, in relation to the reference condition, and in agreement with tensile results reported and discussed by (Kolluri, et al., 2021). In addition, (Kolluri, et al., 2021) showed that the yield and ultimate tensile strength, after irradiation, increase in accordance with the increase of the total Ni+Mn content in the model steels, in the order K, L, M and N. The Vickers hardness results partially follow this trend, with the hardness of irradiated grade K being the lowest, followed by grade L, and grades M and N presenting the highest hardness values, but with no difference between them. Since dislocation loops could not be imaged with the TEM used in the present work, it is not possible to calculate their contribution to irradiation hardening of the steels. Solute clusters rich in Mn-Ni-Si are expected to be present in the model steels at densities that increase with the Ni content of the alloy. These clusters can be characterised with techniques as Atom Probe Tomography and Small Angle Neutron Scattering. The solute clusters and dislocation loops, to be present at densities of the order of 10^{23} and 10^{20} m^{-3} (Almirall, et al., 2019), (Fujita, et al., 2022), respectively, are likely the main contributors to irradiation hardening and suppress the effect of Mo-rich nanosized precipitates observed in higher amount in the materials after irradiation. Evidence for this affirmation is the Vickers hardness of irradiated model steel grade K, which is the lowest, despite being the grade with highest planar density of Mo-rich precipitates after irradiation.

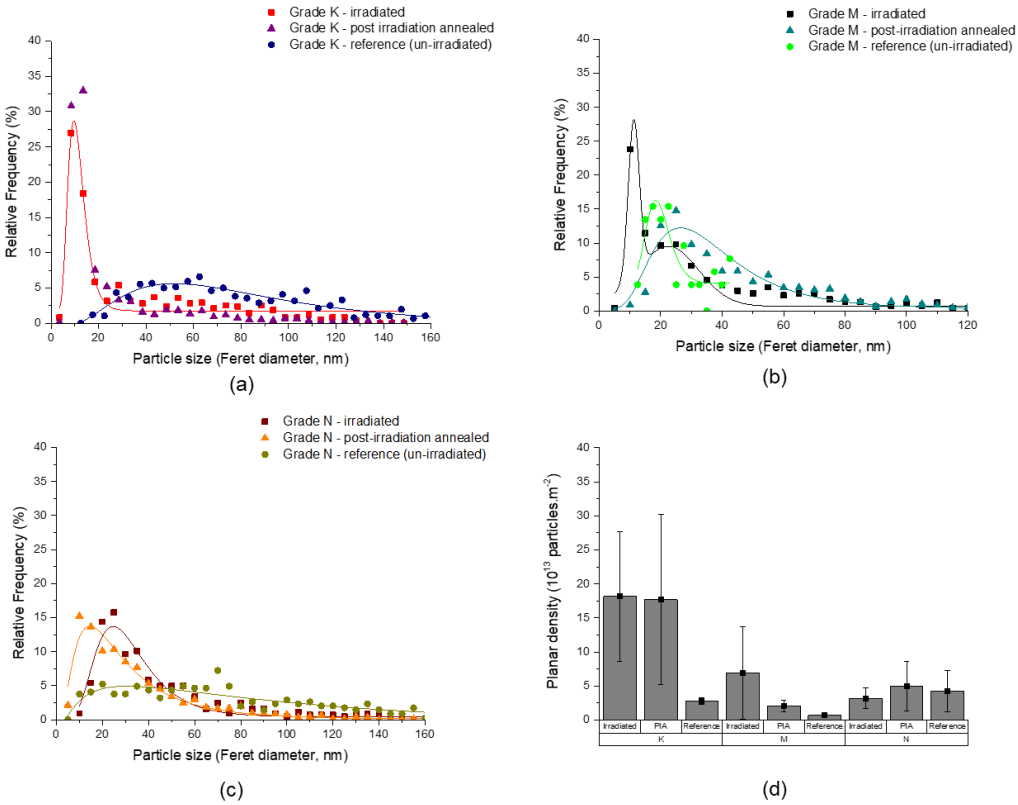

Figure 8. Particle size distributions calculated for model steels (a) grade K, (b) grade M, (c) grade N. (d) Planar density of nanosized particles observed inside grains of the respective model steels.

The average Vickers hardness measured for model steel grade M in reference condition is in contradiction to its observed microstructure. Model steel M has no Fe-rich precipitates at grain boundaries and presents the lowest planar density of Mo-rich precipitates, still, showed the highest hardness in reference condition. All samples used for microscopy were extracted from multiple broken tensile and KLST specimens, and Vickers hardness was measured on fracture toughness samples. A possibility is that heterogeneity in the steel plate used to fabricate the specimens lead to this behavior, and microstructural characterization of the specimens used for Vickers hardness can confirm the hypothesis.

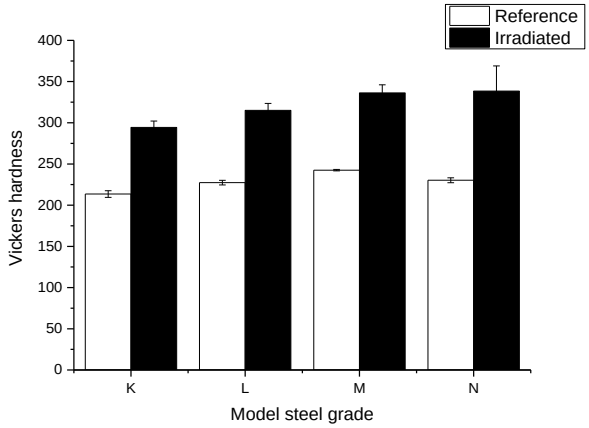

Figure 9. Vickers hardness of model steels K, L, M and N in reference and irradiated conditions.

The effect of PIA at 450 ºC for 40 h on the recovery of mechanical properties of model steels K, L, M and N was previously studied within the STRUMAT-LTO framework, the results were reported and discussed by (Laot, et al., 2022). The post-irradiation annealing treatment proved to be effective in restoring the yield strength (YS) and ultimate tensile strength (UTS) to 75 to 95% of its original values, depending on the steel grade. Steel grade K had 75% recovery in YS and 78% in UTS, steel grade L presented the same degree of recovery as grade K, steel grade M showed 78% recovery in YS and 95% recovery in UTS and, finally, grade N showed 88% recovery in YS and 90% recovery in UTS. Similarly to the irradiated condition, it is not possible to make a proper correlation between the observations made with the TEM and the mechanical testing results. It is known from literature that post-annealing irradiation leads to dissolution of the Ni-Mn-Si solute clusters and annealing out of dislocation loops, but their contributions cannot be quantified here. It is interesting to point out, though, that grade M was the only one to show a particle size distribution in PIA condition closer to its reference condition and was the only grade to show a reduction in planar density of Mo-rich precipitates with PIA, in comparison to irradiated condition. The recovery of UTS measured for grade M after PIA was the highest, which could indicate a role for the Mo-rich precipitates.

CONCLUSIONS

The western PWR model steels K, L, M and N in reference, irradiated and PIA at 450 ºC for 40 h conditions were investigated using microscopy techniques, dilatometry and Vickers hardness. The steels have a complex microstructure in reference condition, composed of mixture of tempered martensite and bainite, Fe-rich sub-micrometric precipitates at grain boundaries and Mo-rich nanosized precipitates inside grains, with the exception of grade M that does not present precipitates at grain boundaries. Dislocation loops could not be imaged in the irradiated specimens, mainly due to technical limitations of the TEM used. Further analysis of these irradiated specimens will be carried out with a more suitable microscope. A surprising result was the observation of the increased fraction of Mo-rich precipitates in the irradiated condition. Model steel grades K and L were the ones presenting highest planar densities of these precipitates after irradiation, followed by grades M and N. In addition, precipitation of Fe-rich sub-micrometric particles occurred at the grain boundaries of model steel M during irradiation. The precipitation behaviour of the model steels is odd and needs to be better

understood. The Vickers hardness results showed the clear hardening of the model steels after irradiation, and is in agreement with tensile testing results reported previously. However, their proper correlation with defect structure could not be completely made due to the impossibility to image dislocation loops.

ACKNOWLEDGEMENTS

The research reported in the project is performed within the framework of the STRUMAT-LTO project. This project has received funding from the Euratom research and training programme 2019–2020 under grant agreement n◦ 945272. The work performed at NRG is co-funded by the Dutch Ministry of Economic Affairs (EZS). The contribution of all partners in the STRUMAT-LTO project is acknowledged.

EXPORT CONTROL NOTE

The content within this document is classified with the code EU DuC = X. EU DuC means European dual use code.

REFERENCES

Almirall, N. et al., 2019. On the elevated temperature stability of nanoscale Mn-Ni-Si precipitates formed at lower temperature in highly irradiated reactor pressure vessel steels. *Nature*, Volume 9.

Bonny, G. et al., 2013. On the thermal stability of late blooming phases in reactor pressure vessel steels: an atomistic study. *Journal of Nuclear Materials*, Volume 442, pp. 282-291.

Fujita, T. et al., 2022. Contribution of dislocation loop to radiation-hardening of RPV steels studied by STEM-EDS with surveillance test pieces. *Journal of Nuclear Materials*, Volume 572, p. 154055.

Kolluri, M., 2023. STRUMAT-LTO: STRUctural MATerials research for safe long-term operation of LWR nuclear power plants. *The Innovation Platform*, March, p. 3.

Kolluri, M. et al., 2021. Influence of Ni-Mn contents on the embrittlement of PWR RPV model steels irradiated to high fluence values relevant for LTO beyond 60 years. *Journal of Nuclear Materials*, Volume 553, p. 153036.

Laot, M. et al., 2022. Effectiveness of thermal annealing in recovery of tensile properties of compositionally tailored PWR model steels irradiated in LYRA-10. *Metals*, p. 904.

Odette, G., 2009. Predictive reactor pressure vessel steel irradiation embrittlement models: Issues and opportunities. *JOM*, 61(7), pp. 17-23.

Odette, G. & Lucas, G., 1998. Recent progress in understanding reactor pressure vessel steel embrittlement. *Radiation Effects and Defects in Solids*, Volume 144, pp. 189-231.

Shimodaira, M. et al., 2018. Contribution of irradiation-induced defects to hardening of a low-copper reactore pressure vessel steel. *Acta Materialia*, Volume 155, pp. 402-409.

Waterschoot, T., Verbeken, K. & De Cooman, B., 2006. Tempering kinetics of the martensitic phase in DP steel. *ISIJ International*, pp. 138-146.

Wells, P. et al., 2014. Evolution of manganese-nickel-silicon-dominated phases in highly irradiated reactor pressure vessel steels. *Acta Materialia*, Volume 80, pp. 205-219.